

# Origins of Stator Current Spectra in DFIGs with Winding Faults and Excitation Asymmetries

S. Williamson\* and S. Djurović†

\* University of Surrey, Guildford, Surrey GU2 7XH, United Kingdom

† School of Electrical and Electronic Engineering, The University of Manchester,  
P.O. Box 88, Sackville Street, Manchester M60 1QD, United Kingdom

**Abstract-** In this paper the authors derive simple expressions for the frequencies of the harmonic components in the steady state stator line current of a DFIG operating under various conditions of supply and/or winding unbalance. The underlying purpose of the work is to identify signature frequencies which may be used in condition monitoring instrumentation to both identify and discriminate between a range of likely faults that may arise in practice. The analytical expressions are verified first by comparison with the spectra calculated using an advanced time-stepped circuit model, and then by comparison with measurements made on an experimental test rig.

## I. INTRODUCTION

Doubly-fed induction generators (DFIGs) are the preferred choice for contemporary large variable speed wind turbines [1,2] due to the advantages they offer over other conventional generator topologies, primarily in terms of power flow control, electromechanical damping and constant output frequency. Maintenance of these machines is rapidly gaining importance in the wind industry. The results of various studies have indicated that winding faults represent one of the most significant causes of induction machine failure [3,4]. The commonly employed techniques for detecting the asymmetry arising from winding faults are for the most part based on exploring the steady state frequency spectra of certain measurable quantities and searching for fault-specific harmonic components. In this respect, line current is the preferred medium [5,6]. Consequently, the analysis of the operation of a DFIG with winding faults has recently received increased attention.

Several authors have examined DFIG current frequency spectra in an attempt to identify an efficient means for condition monitoring [7-12]. The work published to date, however, is mostly based on the analysis of experimental results [7,9]. It does not, for the most part, present an explanation of the origins of the DFIG current spectra nor does it provide expressions for the defined harmonic signatures [7-9]. Additionally some of the methods employed may prove to be unreliable as they are sensitive to inherent machine asymmetry and DFIG unbalanced supply operation, which is a common occurrence during regular generator operation [7,10,11]. Furthermore the modeling approach taken in [10,11] does not paint a complete picture of the current spectra as it accounts for fundamental fields only. In [12] a more advanced analysis of the rotor current spectra is presented with a theoretical explanation of the induction of stator fault related

harmonics in the rotor circuit. The work is confirmed experimentally by identifying harmonic components in the rotor current spectra. However, these are shown to be difficult to extract without invasive monitoring tools due to their small magnitude. In addition the theoretical approach taken in [12] is limited to fault specific harmonic content and offers no explanation of the source of other components found in the spectrum, i.e. it does not discriminate between the frequencies of the harmonic components present in the healthy DFIG current spectrum and those of the fault-induced components.

The available literature indicates that there is a distinct lack of information on the DFIG stator current harmonic content. A detailed analysis of the origins of the spectral content of the stator current would therefore prove beneficial for the design of an efficient DFIG condition monitoring system. This work aims to present a comprehensive theoretical analysis of the DFIG stator current spectrum content for the machine operating in steady state, both with and without supply and/or winding asymmetries. The purpose of this analysis is to establish an understanding of the phenomena that give rise to harmonic components found in the DFIG current spectrum, as well as to investigate the possibility of using relatively simple expressions for the frequencies to seek when performing current spectral analysis. The method yields a series of compact expressions that identify the stator current harmonic components that are produced by any of the operating conditions examined. These analytical expressions are first verified using a time-stepped coupled-circuit model and then by experimental measurement on a specially-constructed test rig.

## II. OUTLINE DESCRIPTION OF THE TIME-STEPPED MODEL AND THE EXPERIMENTAL APPARATUS

The time-stepped DFIG model used in this work is based on the established concepts of coupled-circuit theory and complex conductor distributions [13]. These methods account for higher order air-gap field space harmonics when evaluating winding inductances, and also take into consideration precise winding conductor distributions. This technique is conveniently incorporated into a mathematical model comprising of a standard set of DFIG electromagnetic and mechanical equations, which are solved in a time stepping numerical procedure. The developed model has been extensively verified against measurements obtained from a purpose designed test-

rig that enables the experimental simulation of various DFIG operating conditions.

The laboratory rig emulates a typical wind power DFIG drive. It comprises of a wound rotor induction machine mechanically coupled by a common shaft to a DC motor that acts as a prime mover, i.e. mimics the role of the turbine in a windmill. The wound rotor induction machine rotor circuit is excited by an active front-end converter capable of accommodating bi-directional power flow. The DFIG electrical quantities are measured on the rig using power analyzers installed in the stator and rotor circuit and speed and torque transducers mounted on the shaft; the currents are recorded using a precision digital oscilloscope. The stator coils are brought out to a patch-panel, which facilitates their interconnection, allowing a range of stator winding configurations, both balanced and unbalanced, to be examined experimentally. This setup also enables the experimental investigation of rotor winding unbalance, which is achieved by electromagnetically reversing the roles of primary and secondary windings.

Detailed model and rig descriptions can be found in [14,15], along with comparisons between measurement and time-stepped model predictions.

### III. ANALYSIS

#### A. Air-gap Fields and Induced EMFs

The analysis in this section is based on a three-phase  $2p$ -pole DFIG. The stator winding of this machine is excited at frequency  $\omega$ , whilst its rotor rotates at speed  $\omega_r$  and is excited at frequency  $s\omega$ , where

$$\omega_r = (1-s)\frac{\omega}{p} \quad (1)$$

The rotor of a DFIG is cylindrical, and in this work will be assumed to be mounted concentrically in the stator bore. The stator-driven field will therefore induce only supply-frequency emfs in the stator windings. Non supply-frequency emfs induced in the stator must be produced by fields driven by the currents flowing in the rotor, assuming that the effects of saturation can be ignored. There are two sources of rotor current; the rotor excitation and the emf induced in the rotor by the stator-driven air-gap field. These will be considered in turn.

##### A.1. Rotor-driven fields produced by the rotor excitation current

The air-gap field produced by the rotor excitation will have the general form

$$b_{gr}(\theta', t) = \Re e \left[ \sum_v \sqrt{2} \bar{B}_{gr}^v e^{j(s\omega t - v\theta')} \right] \quad (2)$$

$\theta'$  is an angular co-ordinate measured in a co-ordinate system fixed to the rotor. At this stage we wish to place no restriction on the pole numbers,  $v$ , other than that they are non-zero signed integers. The transformation between the rotor co-ordinate system and that fixed to the stator ( $\theta$ ), is given by

$$\theta = \theta' + \omega_r t \quad (3)$$

The rotor driven air-gap field may now be expressed in the stator reference frame by substituting from (1) and (3) into (2)

$$b_{gr}(\theta, t) = \Re e \left[ \sum_v \sqrt{2} \bar{B}_{gr}^v e^{j \left[ \left( s + \frac{v}{p}(1-s) \right) \omega t - v\theta \right]} \right] \quad (4)$$

Each of these rotating flux waves will induce an emf in the stator conductors at the corresponding frequency,

$$\omega_{ind}^v = \left| s + \frac{v}{p}(1-s) \right| \omega \quad (5)$$

For currents not to flow in the windings at this frequency, the individual conductor emfs must sum to zero across the winding.

##### A.2. Rotor-driven fields produced by currents induced in the rotor

Currents may also be induced in the rotor as a consequence of the air-gap fields produced by the stator excitation. Such fields have the general form

$$b_{gs}(\theta, t) = \Re e \left[ \sum_v \sqrt{2} \bar{B}_{gs}^v e^{j(\omega t - v\theta)} \right] \quad (6)$$

In the rotor reference frame these become,

$$b_{gs}(\theta', t) = \Re e \left[ \sum_v \sqrt{2} \bar{B}_{gs}^v e^{j \left[ \left( 1 - \frac{v}{p}(1-s) \right) \omega t - v\theta' \right]} \right] \quad (7)$$

Each of these rotating flux waves will induce emfs in the rotor conductors. The magnitudes of the resulting rotor winding emfs will depend on the configuration of the rotor windings, and the rotor currents they drive will depend on the impedance of the rotor supply. However, at this stage in the development we will assume that all of the fields in (7) are able to induce currents in the rotor winding. The distribution of the air-gap fields produced by these induced currents depends on the configuration and interconnection of the rotor windings. Each harmonic component of the induced rotor current can set up a spectrum of air-gap fields with different numbers of poles. The rotor-driven flux density produced by the induced rotor currents therefore has the general form

$$b_{gr,ind}(\theta', t) = \Re e \left[ \sum_{\mu} \sum_{\nu} \sqrt{2} \bar{B}_{gr,ind}^{\nu, \mu} e^{j \left[ \left(1 - \frac{\nu}{p}(1-s)\right) \omega t - \mu \theta' \right]} \right] \quad (8)$$

Again, no restriction is placed on the pole-pair number,  $\mu$ , other than to state that they are non-zero integers. Equation (8) expresses the flux density wave produced by the induced rotor currents, in the rotor reference frame. Transferring this into the stator reference frame produces,

$$b_{gr,ind}(\theta, t) = \Re e \left[ \sum_{\mu} \sum_{\nu} \sqrt{2} \bar{B}_{gr,ind}^{\nu, \mu} e^{j \left[ \left\{ 1 - \frac{(\nu - \mu)}{p}(1-s) \right\} \omega t - \mu \theta \right]} \right] \quad (9)$$

Equation (9) shows that the emfs induced in the stator windings due to the currents induced in the rotor windings, will have frequencies given by,

$$\omega_{ind}^{\nu, \mu} = \left| 1 + \frac{\nu - \mu}{p}(1-s) \right| \omega \quad (10)$$

Equations (5) and (10) may be used to derive simple expressions for the emfs induced in the stator windings under a range of operating conditions.

#### B. Machine operating normally

For a machine with no winding faults and balanced excitation on the stator and rotor,  $\nu$  and  $\mu$  have the same form

$$\nu, \mu = p(1 - 6m), \quad m = 0, \pm 1, \pm 2, \pm 3 \dots \quad (11)$$

Substituting these expressions into either (5) or (10), and simplifying gives

$$\omega_{ind}^k = |6k(1-s) \pm 1| \omega, \quad k = 0, 1, 2, 3 \dots \quad (12)$$

$k=0$  corresponds to the stator excitation frequency. Non-zero values of  $k$  relate to speed-dependant high-frequency components of emf which are induced in the stator of a 'healthy' DFIG operating under ideal balanced supply conditions.

#### C. Machine operating with asymmetry on the rotor side

##### C.1. Rotor windings balanced. Rotor excitation unbalanced

An un-balanced rotor excitation will produce air-gap fields with pole-pair numbers given by

$$\nu = \pm p(1 - 6m) \quad m = 0, \pm 1, \pm 2, \pm 3 \dots \quad (13)$$

The positive sign in (13) gives values of  $\nu$  corresponding to (11), and will therefore result in frequencies of induced emf

given by (12). The negative sign, on the other hand, after substitution into (5), results in frequencies given by

$$\omega_{ind}^k = |6k(1-s) \pm (1-2s)| \omega, \quad k = 0, 1, 2 \dots \quad (14)$$

Additional field components will be produced by the rotor if a zero-sequence voltage, produced by the supply unbalance, is able to drive zero-sequence currents through the rotor windings. This would require the rotor to be star-connected, with the star point connected to neutral. The authors do not believe that such a configuration is commonly used, and this option will be neglected.

##### C.2. Rotor windings unbalanced. Rotor excitation balanced

A rotor winding fault has the effect of introducing asymmetry into the rotor mmf pattern. As a consequence, the resulting rotor-driven air-gap field may now contain sub-harmonic pole numbers, i.e.

$$\nu = 1 - 2m, \quad m = 0, \pm 1, \pm 2, \pm 3 \dots \quad (15)$$

If the stator windings are series-connected, the stator will be able to respond only to those harmonic fields which have the same pole numbers as those produced by the stator winding itself (i.e. those pole numbers indicated by (13)). Under such circumstances the emfs induced in the stator windings will have the frequencies given by (12) and (14).

If the stator windings are parallel-connected, however, the stator may be able to respond to some of the sub-harmonic fields. For example, with two parallel paths in the stator, the windings may be capable of having emfs induced by fields with any odd number of pole pairs. Substituting (15) into (5) gives,

$$\omega_{ind}^k = \left| \frac{2k}{p}(1-s) \pm \left[ s + \frac{1-s}{p} \right] \right| \omega \quad (16)$$

#### D. Machine operating with asymmetry on the stator side

##### D.1. Stator winding balanced. Stator excitation unbalanced

Under these circumstances the stator produces fields with pole-pair numbers given by (13). The response of the rotor to these fields is to produce the same pole-pair numbers, with the same sign. That is, when  $\nu$  has the form  $+p(1-6m)$ ,  $\mu$  has the form  $+p(1-6n)$ , where  $m$  and  $n$  are signed integers. And when  $\nu$  has the form  $-p(1-6m)$ ,  $\mu$  has the form  $-p(1-6n)$ . Substitution of these two alternatives into (10) produces the frequencies given by (12). That is, stator excitation asymmetry does not introduce any components into the stator current spectrum that are not present in a 'healthy' machine with a balanced supply.

##### D.2. Stator windings unbalanced. Stator excitation balanced

A stator winding fault has the effect of introducing asymmetry into the stator mmf pattern. As a consequence, the

resulting stator-driven air-gap fields may now contain all pole numbers. The response of the rotor to this harmonic-rich air-gap field will depend on the layout of the rotor windings.

If the rotor windings are series-connected, only those fields which have pole-pair numbers given by  $\nu = \pm p(1-6m)$  will be able to induce non-zero sequence emfs in the rotor. This is analogous to the situation discussed in *D.1.* where it is argued that the frequencies of the stator induced emf spectra will be given by (12). That is, an open-circuit or short-circuit fault on the stator will not result in additional components of induced emf in the stator.

If, on other hand, the rotor windings contain (say) two parallel paths, those stator-driven fields which have odd numbers of pole pairs will also couple with the rotor. That is,  $\nu = 2m + 1$ , where  $m = 0, \pm 1, \pm 2, \pm 3 \dots$ . The rotor's response to these induced emfs will be to introduce fields with the same range of pole numbers, i.e.  $\mu = 2n + 1$ , where  $n = 0, \pm 1, \pm 2, \pm 3 \dots$ . Substituting these two expressions into (7), and simplifying,

$$\omega_{ind}^k = \left| \frac{2k}{p}(1-s) \pm 1 \right| \omega \quad k=0, 1, 2, 3 \dots \quad (17)$$

A summary of the analytical expressions derived in this section is given in Table I.

#### IV. MODEL STUDY

The first step in the verification of the expressions given in Table 1 was accomplished by means of the DFIG time stepping model, which was used to simulate each of the five conditions listed in the table. The purpose of this work was to verify the developed equations through comparison with the predictions from a verified analytical model.

DFIG operation for all possible combinations of supply and winding unbalance was investigated here, equivalent to the

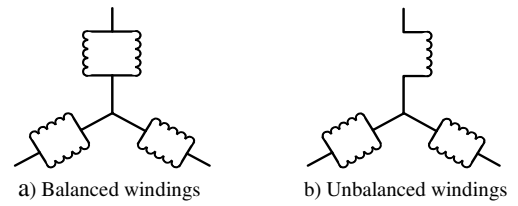


Figure 1. Healthy and faulty winding configurations

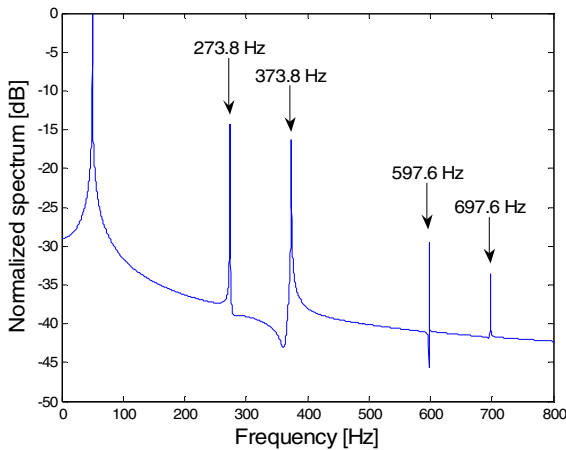
operating scenarios examined in the previous section. These are:

1. Balanced stator and rotor windings;  
Balanced stator and rotor supply.
2. Balanced stator and rotor windings;  
Unbalanced rotor supply, balanced stator supply.
3. Unbalanced rotor windings, balanced stator windings;  
Balanced stator and rotor supply.
4. Balanced stator and rotor windings;  
Unbalanced stator supply, balanced rotor supply.
5. Unbalanced stator windings, balanced rotor windings;  
Balanced stator and rotor supply.

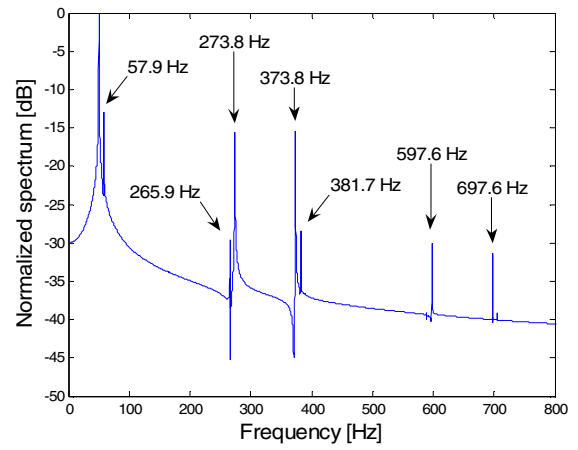
The model study was carried out for a super-synchronous operating speed of *1619 rpm* and a load torque of *24.9 Nm*, which corresponded to test rig measurements performed for the winding configurations shown in Fig. 1. Balanced windings in this work comprise of two winding groups connected in parallel per phase. Winding unbalance is achieved by open circuiting one of the parallel legs in a phase winding. The values of stator and rotor excitation used in the time-stepped simulation calculations were set to be equal to those measured during the experiments. The only exception to this was when balanced supply conditions were under examination, because complete supply balance could not be achieved in the laboratory.

TABLE I  
STEADY STATE STATOR CURRENT HARMONIC FREQUENCIES FOR VARIOUS BALANCED/UNBALANCED SUPPLY AND WINDINGS OPERATING CONDITIONS

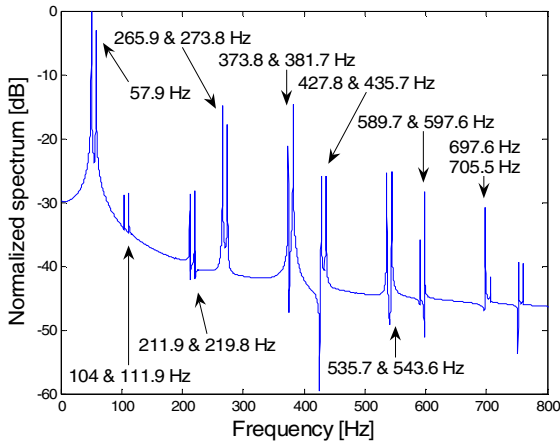
WINDINGS		SUPPLY		INDUCED DFIG STATOR CURRENT FREQUENCIES
STATOR	ROTOR	STATOR	ROTOR	
BALANCED	BALANCED	BALANCED	BALANCED	$f_{ind}^k =  6k(1-s) \pm 1  f$
BALANCED	BALANCED	BALANCED	UNBALANCED	$f_{ind}^k =  6k(1-s) \pm 1  f$ $f_{ind}^k =  6k(1-s) \pm (1-2s)  f$
BALANCED	UNBALANCED	BALANCED	BALANCED	$f_{ind}^k = \left  \frac{2k}{p}(1-s) \pm \left[ s + \frac{1-s}{p} \right] \right  f$
BALANCED	BALANCED	UNBALANCED	BALANCED	$f_{ind}^k =  6k(1-s) \pm 1  f$
UNBALANCED	BALANCED	BALANCED	BALANCED	$f_{ind}^k = \left  \frac{2k}{p}(1-s) \pm 1 \right  f$



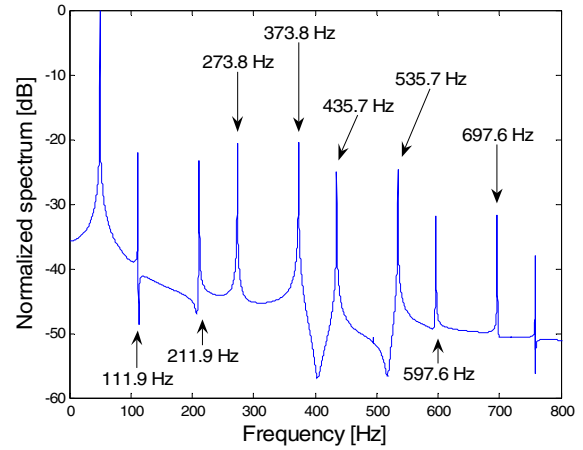
a) Balanced stator and rotor windings,  
Balanced stator and rotor supply



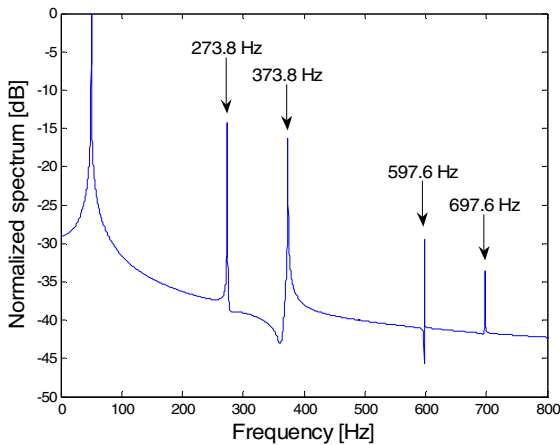
b) Balanced stator and rotor windings,  
Balanced stator and unbalanced rotor supply



c) Balanced stator and unbalanced rotor windings,  
Balanced stator and rotor supply



d) Unbalanced stator and balanced rotor windings,  
Balanced stator and rotor supply



e) Balanced stator and rotor windings,  
Unbalanced stator and balanced rotor supply

Figure 2. Time-stepped model predictions for DFIG current spectrum, 1619 rpm

The excitation voltage used in the time-stepped simulation was represented as consisting of fundamental component only. The supply unbalance introduced on either the stator or the rotor

side is equal to that measured in the laboratory for the experimentally achieved super-synchronous operating point. The steady state mechanical speed value was kept at constant 1619 rpm in the time-stepped simulations for the purpose of this study in accordance with the assumptions made in the analytical work in section III.

Study results for steady state current spectrum are given in Fig. 2 for all of the operating conditions investigated. The magnitudes are normalized with respect to the fundamental harmonic. The bandwidth of data presented is limited to a maximum frequency of 800 Hz as this is the region that the authors found to be most attractive for analysis, due to the relatively high magnitude of spectral components. Frequencies at which the most dominant harmonic components appear in the respective current spectra are labeled in the graphs.

The current spectrum in Fig. 2a for a DFIG operating with balanced windings and balanced excitation is shown to contain four higher order harmonic components, i.e. those shown in the graph at 273.8 Hz, 373.8 Hz, 597.6 Hz and 697.6 Hz. Fig. 2b gives the stator line current spectrum when the machine windings and the stator excitation are balanced, but the rotor

TABLE II  
CALCULATED NUMERIC VALUES OF INDUCED STEADY STATE STATOR CURRENT HARMONIC FREQUENCIES FOR VARIOUS BALANCED/UNBALANCED SUPPLY AND WINDINGS OPERATING CONDITIONS

WINDINGS		SUPPLY		CALCULATED DFIG STATOR CURRENT FREQUENCIES [Hz]		
STATOR	ROTOR	STATOR	ROTOR			
BALANCED	BALANCED	BALANCED	BALANCED	50	273.8	597.6
					373.8	697.6
BALANCED	BALANCED	BALANCED	UNBALANCED	50	373.8	597.6
				57.9	381.7	697.6
				265.9	589.7	705.5
				273.8		
BALANCED	UNBALANCED	BALANCED	BALANCED	50	265.9	535.7
				57.9	273.8	543.6
				104	373.8	589.7
				111.9	381.7	597.6
				211.9	427.8	697.6
				219.8	435.7	705.5
BALANCED	BALANCED	UNBALANCED	BALANCED	50	273.8	597.6
					373.8	697.6
UNBALANCED	BALANCED	BALANCED	BALANCED	50	273.8	535.7
				111.9	373.8	597.6
				211.9	435.7	697.6

supply is not. The spectrum not only contains all of the harmonic components present in Fig. 2a, but also exhibits the presence of additional sideband components at 57.9 Hz, 265.9 Hz and 381.7 Hz. These are clearly produced by the rotor supply unbalance. In the case of a DFIG operating with rotor winding unbalance, balanced stator windings, and balanced excitation on both, Fig. 2c indicates that additional harmonic components of stator current are induced at 57.9 Hz, 104 Hz, 111.9 Hz, 211.9 Hz, 219.8 Hz, 265.9 Hz, 381.7, 427.8 Hz, 435.7 Hz, 535.7 Hz, 543.6 Hz, 589.7 Hz and 705.5 Hz. Again, this spectrum also exhibits the four harmonic components present in a machine operating with balanced windings and excitation. The current spectral content for a DFIG operating with balanced supply and rotor windings and unbalanced stator windings is shown in Fig. 2d to contain additional harmonic components at 111.9 Hz, 211.9 Hz, 435.7 Hz and 537.7 Hz. The four harmonic components observed for machine operation with balanced supply and windings are again seen to be present. Finally, the time-stepped model results shown in Fig. 2e for DFIG operation with unbalanced stator and balanced rotor excitation and with balanced windings, indicate that, the presence of stator excitation asymmetry does not introduce new components in the stator current spectrum. Comparison of Fig. 2e with Fig. 2a shows that no new harmonic components have been introduced.

The stator current harmonic spectra presented in figures 2a-e all exhibit the harmonic components that are present in a machine with balanced windings and excitation. Rotor excitation unbalance, or rotor winding asymmetry are seen to introduce additional frequency components in the stator line current, as does stator winding unbalance. These observations suggest that the presence of certain harmonic components may indeed be used to identify different types of winding or supply asymmetry.

The frequencies of harmonic components induced in the

current spectra at operating speed of 1619 rpm that are predicted by the equations in Table I are listed in Table II. The derived expressions yield a series of possible stator current harmonic frequencies. The magnitudes of these components depend on a number of parameters, including operating speed, winding configuration, and rotor skew. The numeric values listed in Table II are those that match the ones found in the analytical expressions given in Table I. Comparison of the corresponding data in Table II and Fig. 2 demonstrates that the time-stepping model produces harmonic components which accord with the analytical expressions derived in section III. Although the time-stepped model has been validated against measurement, this is still the use of one model to confirm another, and so an experimental investigation was also carried out.

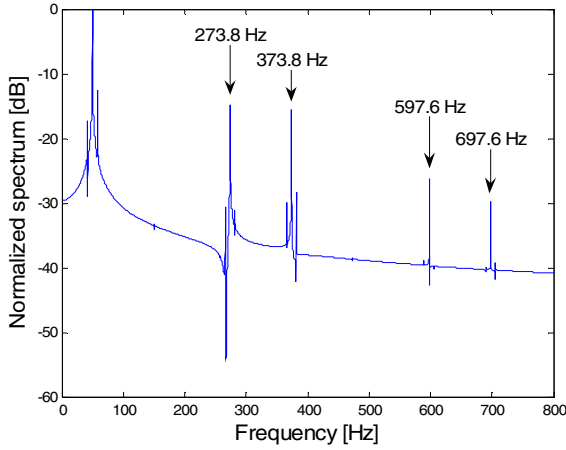
## V. MEASUREMENTS AND PREDICTIONS

In this section we demonstrate the validity of the time-stepped model for the prediction of the frequencies of harmonic currents, by comparing measured and predicted spectra for a range of DFIG winding configurations. The measurements were taken for a machine operating at 1619 rpm with both balanced windings and with an asymmetry present in stator or rotor windings, as shown in Fig. 1. The measured excitation voltages are typically unbalanced and correspond to the asymmetry that exists in the laboratory supply, which was used to generate data in Fig. 2. The excitation and load torque values recorded in the experiments are used as model data inputs in order to credibly represent the operating conditions observed in the laboratory tests. As before, supply voltages are modeled in calculations as fundamental sine waves for the purpose of this analysis. It is also important to point out that the measured current data contains speed ripple effects, as minute speed fluctuations arise due to the electromagnetic

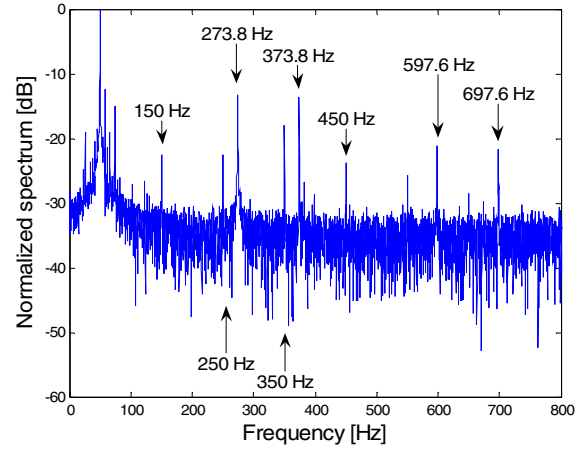
unbalance that is inevitably present in any DFIG drive [16,17]. This phenomenon was reproduced in the model by allowing the mechanical speed to vary in the simulations, i.e. by resolving the model steady state mechanical characteristic for angular speed in each numerical iteration. As both the

theoretical analysis and the model study were performed on the assumption of constant speed the results presented here are also an efficient demonstration of the speed ripple effects on healthy and faulty DFIG line current spectrum.

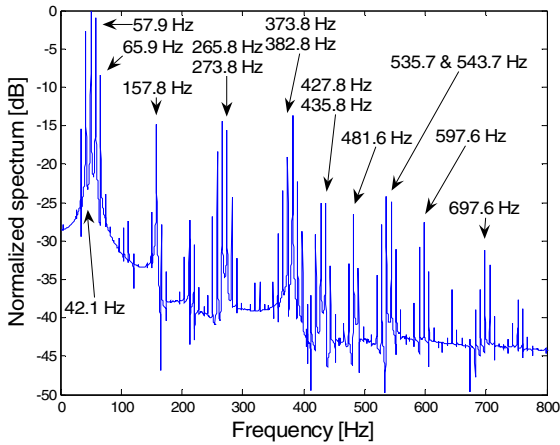
The predicted and measured current spectra for the winding



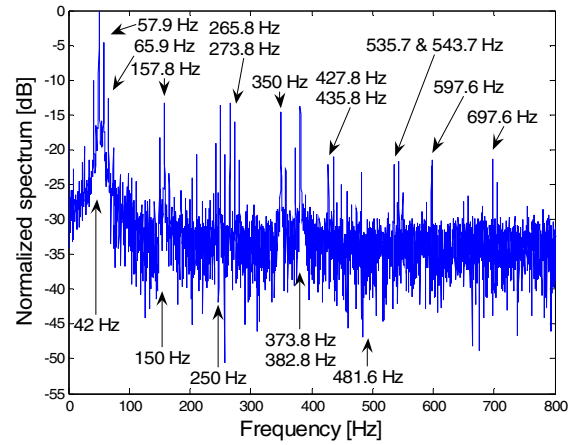
a) Balanced stator and rotor windings, model predictions



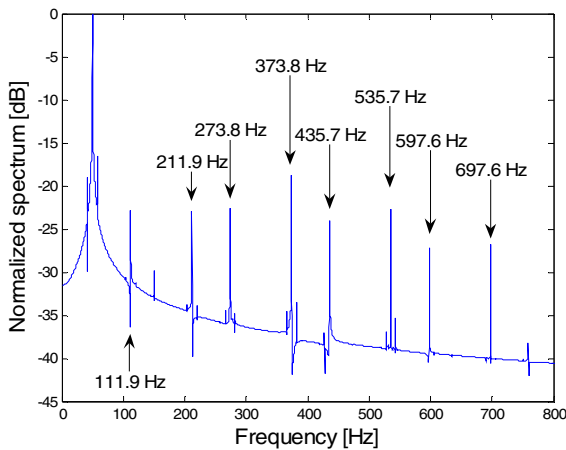
a) Balanced stator and rotor windings, test rig measurement



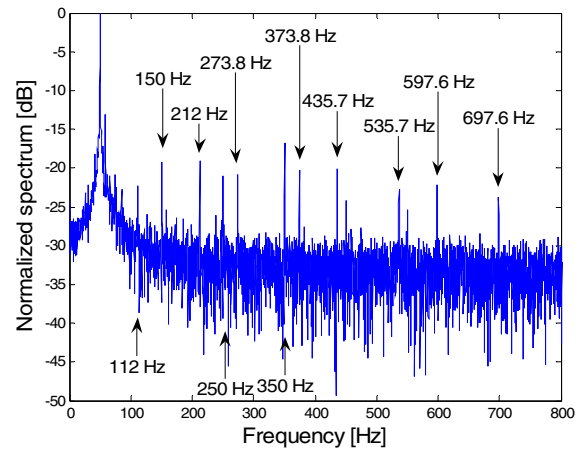
b) Balanced stator and unbalanced rotor windings, model predictions



b) Balanced stator and unbalanced rotor windings, test rig measurement



c) Unbalanced stator and balanced rotor windings, model predictions



c) Unbalanced stator and balanced rotor windings, test rig measurement

Figure 3. Model predictions for DFIG current spectrum, variable speed, 1619 rpm

Figure 4. Test rig measurements for DFIG current spectrum, 1619 rpm

and excitation conditions that have been previously considered are shown in Fig. 3 and Fig. 4, respectively. The corresponding calculated and experimental data sets are seen to be in good agreement when spectral content is concerned. The most dominant frequency components are labeled in the graphs and are clearly identifiable in predictions and measurements alike. Minor discrepancies between some of the measured and predicted harmonic frequency values are due to spectral resolution difference between the simulated and experimental data. In addition, harmonic components that exist in the measured current spectrum at multiples of line frequency (*150 Hz, 250 Hz, 350 Hz...*) typically originate from the higher order harmonic content in the power supply but may also arise from magnetic saturation within the machine. These effects are not accounted for in the model and are thus not present in the calculated spectra. Furthermore the absence of these components in model predictions is expected, since model considerations [14] and the presented theoretical analysis are focused on investigation of the current spectra harmonic components that originate from machine based electromagnetic phenomena. The measured data also exhibit an apparent higher noise level when compared to model calculations. This is induced primarily by the rotor converter switching and is not accounted for in the analytical considerations. The spectra presented in Figs 3 and 4 amply demonstrate the validity of the time-stepped model, which itself has been used to confirm the frequency expressions given in Table I. It is also noticeable, however, that some of the harmonic components of small magnitudes in the predicted spectra are buried in the noise in the experimental data. Furthermore, where results from Fig. 2 and Table II differ from the measured data is in predicting the existence of sideband components, which arise as a result of the speed ripple. It will be recalled by the reader that the speed is assumed to be constant throughout the analysis in sections II and III. It will be shown in a separate paper that speed ripple gives rise to additional sideband components throughout the current spectra in Fig. 3 and Fig. 4, and most prominently to those around fundamental frequency. Other sideband components of lesser magnitude can also be observed at higher frequencies in the spectra. This is especially evident for machine operation with rotor winding unbalance.

## VI. CONCLUSIONS

In this paper the authors have developed a set of simple expressions for the stator line current harmonic frequency components which may be present in a DFIG under a range of operating conditions. The magnitudes of these harmonic components will depend largely on the design of the machine under investigation. Design artifacts such as coil pitch and rotor skew will have an influence on harmonic magnitudes. However, not all will be attenuated, so that the identification of one of the characteristic frequency components may be sufficient to uniquely identify a fault. The expressions have been verified by comparison with the predictions of a time-

stepped coupled-circuit model, which is itself validated using experimental measurements made on a test rig, for a range of operating conditions. The authors believe that work presented in this paper is an important step towards the development of condition-monitoring techniques for DFIGs, and provides a better understanding of the mechanisms that generate particular harmonic frequencies in the stator line current.

## REFERENCES

- [1] Y. Amirat, M.E.H. Benbouzid, B.Bensaker, R.Wamkeue, "Generators for Wind Energy Conversion Systems: State of the art and Coming Attractions", *Journal of Electrical Systems* 3-1, pp 26-38, 2007.
- [2] A.D. Hansen, F.Iov, F. Blaabjerg, L.H.Hansen, "Review of Contemporary Wind Turbine Concepts and their Market Penetration", *Wind Engineering*, vol. 28, Issue 3, pp 247-263, 2004.
- [3] Motor Reliability Working Group, "Report of large motor reliability survey of industrial and commercial installations, Part I", *IEEE Transactions on Industry Applications*, Vol IA-21, No 4, July/August 1985.
- [4] O.V. Thorsen, M. Dalva, "Failure identification and analysis for high-voltage induction motors in the petrochemical industry", *IEEE Transactions on Industry Applications*, Vol 35, No 4, July/August 1995.
- [5] A. Siddique, G.S. Yadava, B. Singh, "A Review of Stator Fault Monitoring Techniques for Induction Motors", *IEEE Transactions on Energy Conversion*, Vol 20, No 1, March 2005.
- [6] M.E.H. Benbouzid, "A review of induction motors signature analysis as a medium for faults detection", *IEEE Transactions on Industrial Electronics*, Vol 47, No 5, October 2000.
- [7] I. Boldea, L.M. Popa, B. Jensen, E. Ritchie, "Condition monitoring of wind generators", *Industry Applications Conference, Conference record of the 38th IAS Annual Meeting*, Vol 3, pp 1839-1846, October 2003.
- [8] Q.F. Lu, Z.T. Cao, E. Ritchie, "Model of stator inter-turn short circuit fault in doubly-fed induction generators for wind turbine", *35th Annual IEEE Power Electronics Specialist Conference*, Vol 2, pp 932-937, June 2004.
- [9] H. Douglas, P. Pillay, P. Barendse, "The detection of inter-turn stator faults in doubly-fed induction generators", *IEEE Industry Applications Conference*, Vol 2, pp 1097-1102, October 2002.
- [10] A. Stefani, A. Yazidi, C. Rossi, F. Fillipeti, D. Casadei, G.A. Capolino, "Doubly fed induction machines diagnosis based on signature analysis of rotor modulating signals", *IEEE Transactions on industry applications*, Vol 44, No 6, November/December 2008.
- [11] D. Casadei, F. Fillipeti, A. Stefani, C. Rossi, A. Yazidi, G.A. Capolino, "Experimental fault characterization of doubly fed induction machines for wind power generation", *International Symposium on Power Electronics, Electrical Drives, Automation and Motion, SPEEDAM*, pp 1281-1286, May 2006.
- [12] D. Shah, S. Nandi, P. Neti, "Stator inter-turn fault detection of doubly-fed induction generators using rotor current and search coil voltage signature analysis", *Conference record of the 2007 IEEE Industry Applications Conference*, pp 1948-1953, September 2007.
- [13] S. Williamson, E.R. Laithwaite, "Generalized harmonic analysis for the steady-state performance of sinusoidally-excited cage induction motors", *IEE Proc.*, Vol. 133, Pt. B, No 3, May 1985.
- [14] S. Djurovic, S. Williamson, A. Renfrew, "Dynamic model for doubly-fed induction generators with unbalanced excitation, both with and without winding faults", *IET Electric Power Applications*, March/April 2009.
- [15] S. Djurovic, S. Williamson, "A coupled-circuit model for a DFIG operating under unbalanced conditions", *Proceedings of IEEE International Conference on Electrical Machines, IECM 2008, Portugal*, September 2008.
- [16] F. Fillipeti, G. Francheschini, C. Tassoni, P. Vas, "AI Techniques in induction machines diagnosis including the speed ripple effect", *IEEE Transactions on Industry Applications*, Vol 34, No 1, January/February 1998.
- [17] Y. Liao, L. Ran, G.A. Putrus, K.S. Smith, "Evaluation of the effects of rotor harmonics in a doubly fed induction generator with harmonic induced speed ripple", *IEEE Transactions on Energy Conversion*, Vol 18, No 4, December 2003.